Japanese Journal of Applied Physics

REGULAR PAPER • OPEN ACCESS

Comparison of field-cooling DC poling and AC poling for lead perovskite relaxor-$PbTiO_3$ single crystals grown by a continuous feeding Bridgman process

To cite this article: Yohachi Yamashita *et al* 2024 *Jpn. J. Appl. Phys.* **63** 04SP37

Japanese Journal of Applied Physics **63**, 04SP37 (2024) **REGULAR PAPER**
https://doi.org/10.35848/1347-4065/ad2fe0

Comparison of field-cooling DC poling and AC poling for lead perovskite relaxor-$PbTiO_3$ single crystals grown by a continuous feeding Bridgman process

Yohachi Yamashita[1,2*], Yushi Yamagata[2], Yu Xiang[2], Hiroshi Maiwa[2], Zhengze Xu[1], and Xiaoning Jiang[1]

[1]Mechanical & Aerospace Engineering, North Carolina State University, Raleigh, NC 27695-7910 United States of America
[2]Human Environmental Department, Shonan Institute of Technology, 1-1-25 Tujido-Nishikaigan, Fujisawa, Kanagawa 251-8511, Japan

*E-mail: sxjwg220@ybb.ne.jp

Received November 9, 2023; revised February 21, 2024; accepted March 4, 2024; published online April 5, 2024

We investigated the effectiveness of poling processes for $Pb(Mg_{1/3}Nb_{2/3})O_3$-$PbTiO_3$ single crystals (SCs) produced using a continuous feeding Bridgman method, which is known to produce a high property uniformity. The four studied poling processes are: (I) standard direct current poling (STD-DCP); (II) low-voltage field-cooling DCP (LV-FCP); (III) high-voltage field-cooling DCP (HV-FCP); and (IV) mid-temperature alternating current poling (MT-ACP). The highest free dielectric constant ($\varepsilon_{33}{}^T/\varepsilon_0$) and piezoelectric constant (d_{33}) were obtained by MT-ACP ($\varepsilon_{33}{}^T/\varepsilon_0 = 11\,000$, $d_{33} = 3000$ pC/N), followed by LV-FCP ($\varepsilon_{33}{}^T/\varepsilon_0 = 7500$, $d_{33} = 2400$ pC/N), HV-FCP ($\varepsilon_{33}{}^T/\varepsilon_0 = 6250$, $d_{33} = 1850$ pC/N), and STD-DCP ($\varepsilon_{33}{}^T/\varepsilon_0 = 6200$, $d_{33} = 1800$ pC/N). The LV-FCP SC showed a 21% and 33% increase in $\varepsilon_{33}{}^T/\varepsilon_0$ and d_{33} compared to that of the STD-DCP SC; however, this was not as much as the 77% and 67% improvement of the MT-ACP SC. These results provide guidance for SC transducers.

1. Introduction

The piezoelectric effect discovered in 1880 by the Curie brothers refers to the electromechanical coupling that converts mechanical energy into electrical energy and vice versa. Piezoelectric devices have since been utilized in various devices such as actuators, medical imaging probes, sensors, and underwater acoustic devices.[1–3] Relaxor-type lead-based perovskite piezoelectric single crystals (SCs) such as binary $Pb(Mg_{1/3}Nb_{2/3})O_3$-$PbTiO_3$ (PMN-PT) and ternary $Pb(In_{1/2}Nb_{1/2})O_3$-PMN-PT have been utilized for these applications.[4–6] Among these applications, ultrasound imaging probes have been taking a center position since early 2000.[7] These relaxer-based SCs have a high free dielectric constant ($\varepsilon_{33}{}^T/\varepsilon_0$) over 5000, a piezoelectric constant (d_{33}) over 1500 pC/N, and a bar-mode electromechanical coupling factor (k_{33}) over 90%, which are significantly higher than those of conventional $Pb(Zr,Ti)O_3$ (PZT) ceramics, and hence are very attractive for high-end ultrasonic transducer applications. These SCs have been mostly manufactured using the one-charge Bridgman (OC-BM) process since their initial development in the early 2000s. However, it has been pointed out that a major problem with OC-BM SCs is that the raw material of TiO_2 content changes significantly within the ingot during SC growth, resulting in a large variation in dielectric and piezoelectric properties of more than 100%.[8–10] In 2011, JFE Minerals Co. Chiba, Japan, succeeded in growing PMN-PT SCs by a continuous feeding Bridgman (CF-BM) method using ceramic raw material pellets feeding that solved the problems of OC-BM SCs.[11] A piezoelectric PMN-0.3PT SC boule with a size of 80 mm in diameter, 320 mm in length, and 13 kg in weight has been produced in the last decade. These CF-BM SCs show very uniform piezoelectric properties, within 10% within and between wafers in the ingot, as shown in Fig. 1.[11–16] Poling procedures for these SCs are essential to obtain high piezoelectric and dielectric properties such as d_{33}, k_{33}, and $\varepsilon_{33}{}^T/\varepsilon_0$. Conventional direct current poling (DCP) with high-temperature field cooling (FCP) has been used since the first discovery of these SCs by Kuwata et al. in 1982 and Shrout et al. in 1990.[17,18] Lin et al. reported that outstanding d_{33} (2200 pC/N) can be obtained by FCP from 260 °C to rRT at 6 kV cm^{-1}, which is superior to DCP at RT ($d_{33} = 1300$ pC/N) for 0.1 mm thick PMN-PT SC.[19] Recently, alternating current poling (ACP), a readily controllable domain engineering method, has attracted many researchers' interest owing to enhanced d_{33} and $\varepsilon_{33}{}^T/\varepsilon_0$.[20–42] However, there is no report on systematic comparisons regarding the effectiveness of FCP and ACP processes for PMN-PT CF-BM SCs with high composition and property uniformity. Therefore, the purpose of this study is to compare the electrical properties of DCP, FCP, and ACP conditions for PMN-0.30PT SCs grown by the CF-BM process.[14,15] Our initial report only disclosed the temperature dependence of the dielectric constant of DCP SCs and did not mention the microstructure of the SCs, which greatly affects piezoelectric and dielectric properties.[43] In this report, we have investigated in detail the electrical properties under four different poling conditions, and their relation to the microstructure is clarified.

2. Experimental methods

Figure 2(a) shows the [011]-seeded and [001]-oriented CF-BM PMN-0.30PT SC of a large plate (L65 × W13 × T0.48 mm^3, coercive field (E_C) = 2.2 kV cm^{-1} at RT), which was sputtered with NiCr/Au (30/200 nm) electrodes on its (001)-surfaces. The large plate SC was depoled at 250 °C for 30 min and was cut into 19 pieces of small plates for this experiment (L3 × W13 mm × T0.48 mm^3), as shown in Fig. 2(b), in order to minimize property variations. Figure 3 shows schematic images of the four poling types: (I) standard (STD)-DCP; (II) low-voltage (LV)-FCP; (III) high-voltage (HV)-FCP; and (IV) mid-temperature (MT)-ACP. In the high-temperature FCP process of (II) and (III), the SCs were poled with poling fields of 3 and 6 kV cm^{-1} at 200 °C for 5 min, and then slowly cooled down to RT under the same poling field at a temperature-controlled electric oven for 1000 min. For (IV), the MT-ACP process, a bipolar voltage of sine waves was generated by a multifunctional synthesizer (NF Electronic Instruments, 1930A, Yokohama, Japan) first, and then amplified by a high-voltage

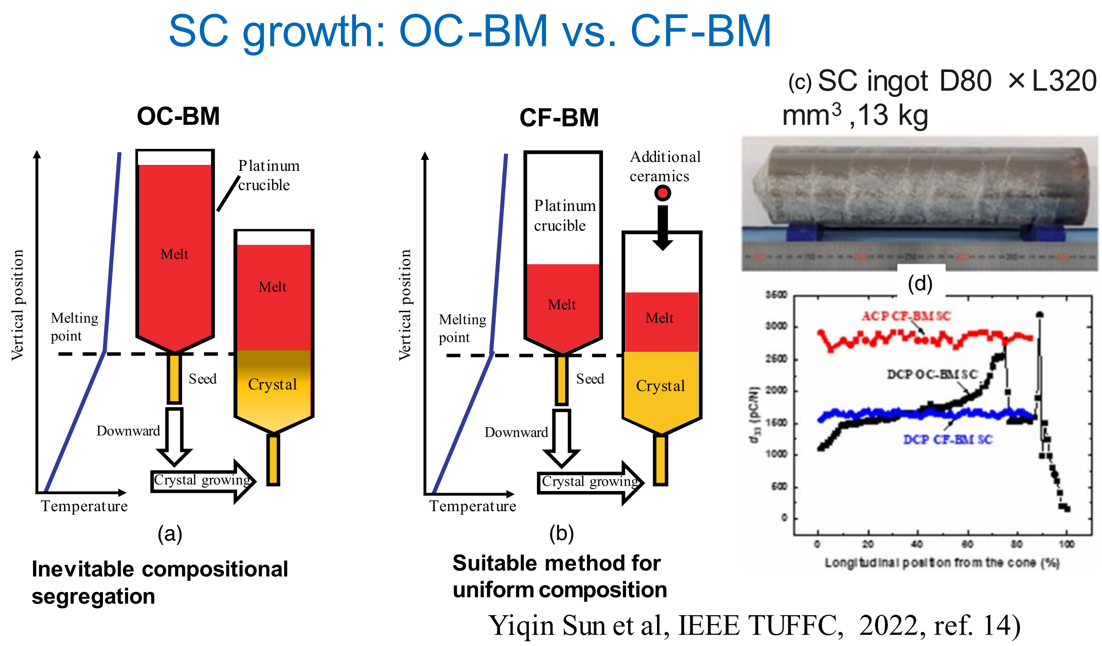

Fig. 1. Schematic images of (a) OC-BM and (b) CF-BM processes, (c) SC ingot, and (d) piezoelectric constant d_{33} distribution within an ingot. Note that the d_{33} distribution of the CF-BM SCs is less than 10% within an ingot.

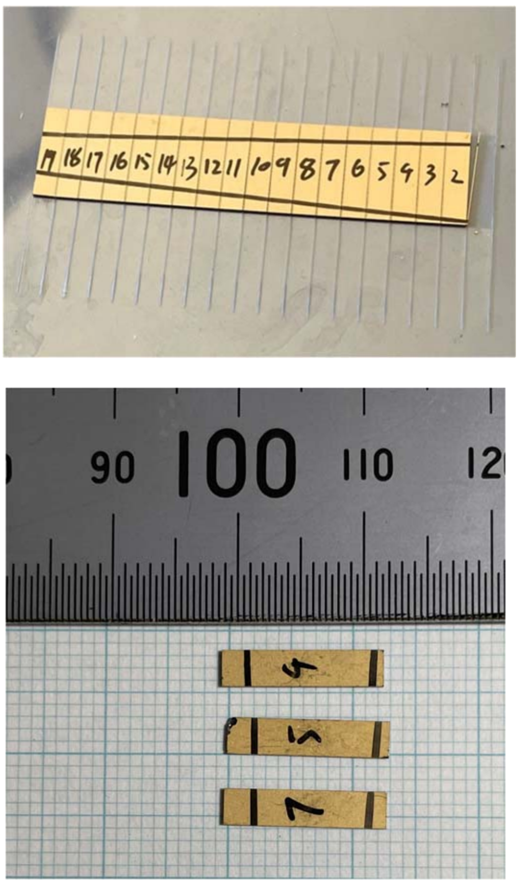

Fig. 2. CF-BM PMN-0.3PT SC samples; the dimension of (a) the initial plate was 65 × 13 × 0.48 mm, and (b) the test sample was 3 × 13 × 0.48 mm, respectively. Note that all evaluated small samples were obtained from one large plate to minimize property distributions between the samples.

amplifier (Trek Inc., 609D-6, CA, USA). The MT-ACP processes were carried out using a bipolar sine wave of 3 kVrms/cm with a frequency of 0.1 Hz for 12 cycles at 60 °C, according to Wan and Sun et al.'s studies.[29,30] The (I) STD-DCP process was conducted at 5 kV cm^{-1} for 1 min according to the Institute of Electrical and Electronics Engineering standard for comparisons.[44] After aging for 48 h after each poling process, the piezoelectric and dielectric properties of the SC samples were evaluated with an impedance analyzer (Agilent Technology, 4194 A, CA, USA) and a piezo d_{33} meter (ZJ-6B, Chinese Academy of Science, Beijing, China).

The temperature dependences of $\varepsilon_{33}{}^{T}/\varepsilon_0$ of the small plate SC samples were measured at 1 kHz using an LF impedance Analyzer (Yokogawa-Hewlett Packar. Ltd., 4192A, Tokyo, Japan).

The $\varepsilon_{33}^{T}/\varepsilon_0$ and clamped dielectric constant ($\varepsilon_{33}^{S}/\varepsilon_0$) were calculated from capacitances measured by the impedance analyzer at 1 kHz and the two times anti-resonant frequency ($2f_a$) of thickness mode k_t, respectively.

As shown in Eq. (1),

$$\frac{\varepsilon_{33}^{T}}{\varepsilon 0} \text{ or } \frac{\varepsilon_{33}^{S}}{\varepsilon 0} = \frac{C \cdot t}{S \cdot \varepsilon_0}, \qquad (1)$$

where C, ε_0, t, and S are capacitance (F), vacuum permittivity of $8.854 \times 10^{-12}\,\mathrm{F\,m^{-1}}$, sample thickness (m), and the sample area (m^2), respectively.

The bar-mode electromechanical coupling factor (k_{33}) was calculated from $\varepsilon_{33}^{T}/\varepsilon_0$ and $\varepsilon_{33}^{S}/\varepsilon_0$, as shown in Eq. (2):

$$k_{33} = \left(\frac{\varepsilon_{33}^{T}/\varepsilon_0 - \varepsilon_{33}^{S}/\varepsilon_0}{\varepsilon_{33}^{T}/\varepsilon_0}\right)^{\frac{1}{2}}. \qquad (2)$$

$\varepsilon_{33}^{T}/\varepsilon_0$ is a free dielectric constant at 1 kHz and $\varepsilon_{33}^{S}/\varepsilon_0$ is a clamped dielectric constant at twice the anti-resonance frequency ($2f_a$). The electromechanical coupling factor thickness mode (k_t) for the plate was calculated from a resonant frequency (f_r) and anti-resonant frequency (f_a) of the fundamental k_t mode, as shown in Eq. (3):

$$k_t = \left(\frac{\pi}{2}\frac{f_r}{f_a}\tan\frac{\pi(f_a - f_r)}{2f_a}\right)^{\frac{1}{2}}. \qquad (3)$$

Frequency constants of the thickness mode (N_t) and length extensional mode N_{31} (Hz·m) were calculated from f_r and t or

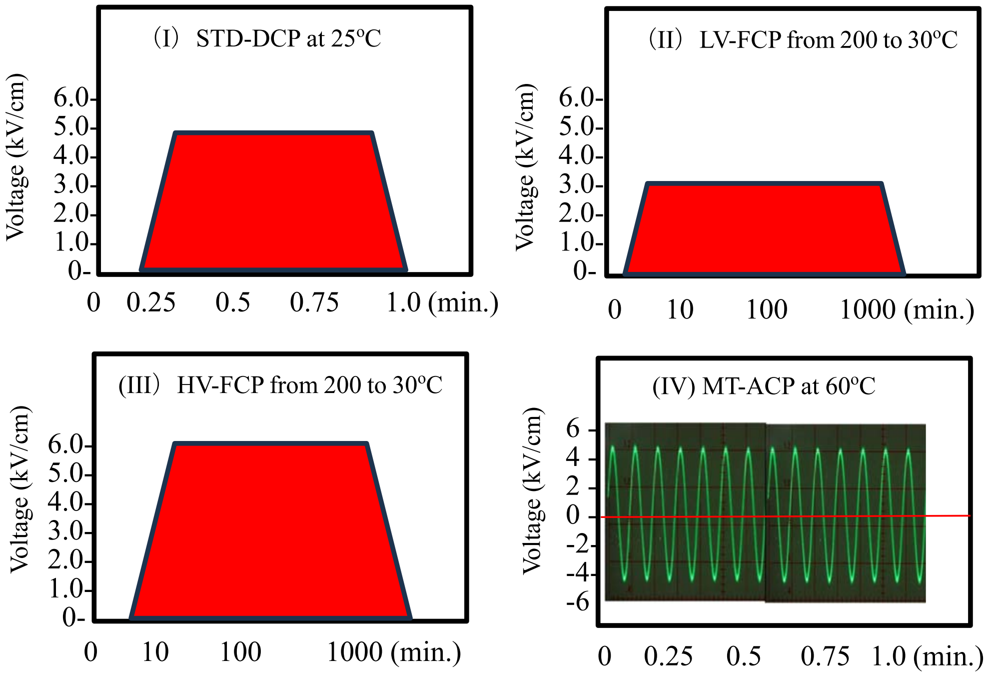

Fig. 3. Schematic images of the four poling processes: (I) STD-DCP; (II) LV-FCP; (III) HV-FCP; and (IV) MT-ACP.

l, where f_r, t, and l are the resonance frequency, sample thickness, and length, respectively. The sound velocity (V) and acoustic impedance (Z_{33}) were also calculated from the k_t mode.

$$\text{Sound velocity } (V) = t \times 2fa(\text{Hz} \cdot \text{m}) \tag{4}$$

$$Z_{33} = V \times \text{density}. \tag{5}$$

Other equations for material property calculations can be found in our previous report.[29)]

At least three sample plates were measured, and average values are used in this work.

3. Results and discussion

Table I shows the poling conditions and the averaged material constants at 25.0 °C for the PMN-0.3PT SCs under the four different poling processes, (I) STD-DCP, (II) LV-FCP, (III) HV-FCP, and (IV) MT-ACP.

Figure 4 shows (a) $\varepsilon_{33}{}^{T}/\varepsilon_0$, (b) $\varepsilon_{33}{}^{S}/\varepsilon_0$, and (c) calculated k_{33} of the PMN-0.3PT SCs under the four different poling processes. The highest $\varepsilon_{33}{}^{T}/\varepsilon_0$ of 11 000 was obtained by the (IV) MT-ACP process, followed by 7500 with the (II) LV-FCP SC, 6250 with the (III) HV-FCP SC, and 6200 with the (I) STD-DCP SC. The $\varepsilon_{33}{}^{T}/\varepsilon_0$ and $\varepsilon_{33}{}^{S}/\varepsilon_0$ of the (II) LV-FCP SC showed 21% and −6% increases compared to those of the (I) STD-DCP SC, respectively; however, this was not as much as the 77% and 18% improvement by the (IV) MT-ACP process.

Figure 5 shows the temperature dependence of $\varepsilon_{33}{}^{T}/\varepsilon_0$ (a) from RT to 200 °C, (b) from 25 to 115 °C, and (c) these $\varepsilon_{33}{}^{T}/\varepsilon_0$ of 50 °C decreased from the phase change temperature (Tpc) for the PMN-0.3PT SCs for the different poling processes. Material constants for ordinary piezoelectric SCs are measured at RT, from about 20 to 25 °C. The material constants in Table I in this paper were obtained from measurements at different RT, e.g., from 17 °C in winter to 28 °C in summer, all calculated at 25 °C using temperature correction factors, 1.0%/ °C, of the PMN-0.3PT SCs. The PMN-0.3PT SCs have a high $\varepsilon_{33}{}^{T}/\varepsilon_0 > 12\,000$ and d_{33} at the Tpc compared to those of RT. The temperature coefficients of $\varepsilon_{33}{}^{T}/\varepsilon_0$ and d_{33} of the SC material are about 1%/ °C, which is considerably larger than the 0.3%–0.8%/ °C of commercially available PZT ceramics. Therefore, high $\varepsilon_{33}{}^{T}/\varepsilon_0$ and d_{33} can be easily obtained at RT by lowering the Tpc of piezoelectric SC below 65 °C. The PMN-30PT SC with Sm doping reported by Li et al. in 2019 showed an RT $\varepsilon_{33}{}^{T}/\varepsilon_0$ of 12 000 and d_{33} of 4100 pc N^{-1}. However, the Tpc of this SC is

Table I. Poling conditions and material constants of PMN-0.3PT SCs for the four poling processes, (I) STD-DCP, (II) LV-FCP, (III) HV-FCP, and (IV) MT-ACP.

Poling processs	(I) STD-DCP	(II) LV-FCP	(III) HV-FCP	(IV) MT-ACP
Poling voltage (kV/cm)	5	3	6	3
Poling temperature (°C)	25	200–30	200–30	60
Poling time (min.)	1	1000	1000	2
$\varepsilon_{33}{}^{T}/\varepsilon_0$	6200	7500	6250	11 000
$\varepsilon_{33}{}^{S}/\varepsilon_0$	1140	1080	980	1350
$\varepsilon_{33}{}^{T}/\varepsilon_0$ at a 50 °C decrease from the Tpc	6880	7670	6470	12 500
Dielectric loss (%)	0.38	0.25	0.3	0.27
Calculated k_{33} (%)	90	92.8	91.8	93.3
k_t (%)	59.5	60	58	60.5
N_t (Hz•m)	1915	1910	1913	1920
k_{31} (%)	45	53.5	55	47
N_{31} (Hz•m)	770	605	630	570
Sound velocity (m/sec.)	4580	4580	4560	4560
d_{33} (pC/N)	1800	2400	1850	3000
g_{33} (10^{-3}Vm/N)	32.8	36.1	33.4	30.8
$S_{33}{}^{E}$ (10^{-12}m^2/N)	54.8	(80)*	(55)**	101.8
Z_{33} (Mrayls)	37.1	37.1	37.0	37.0
Tpc1 (°C)	88	76	75	87
Tpc2 (°C)		91	93	101
Tc (°C)	143	143	143	143
Tm (°C)	150	150	150	150

*, ** These $S_{33}{}^{E}$ were estimated from the data of (I) and (IV).

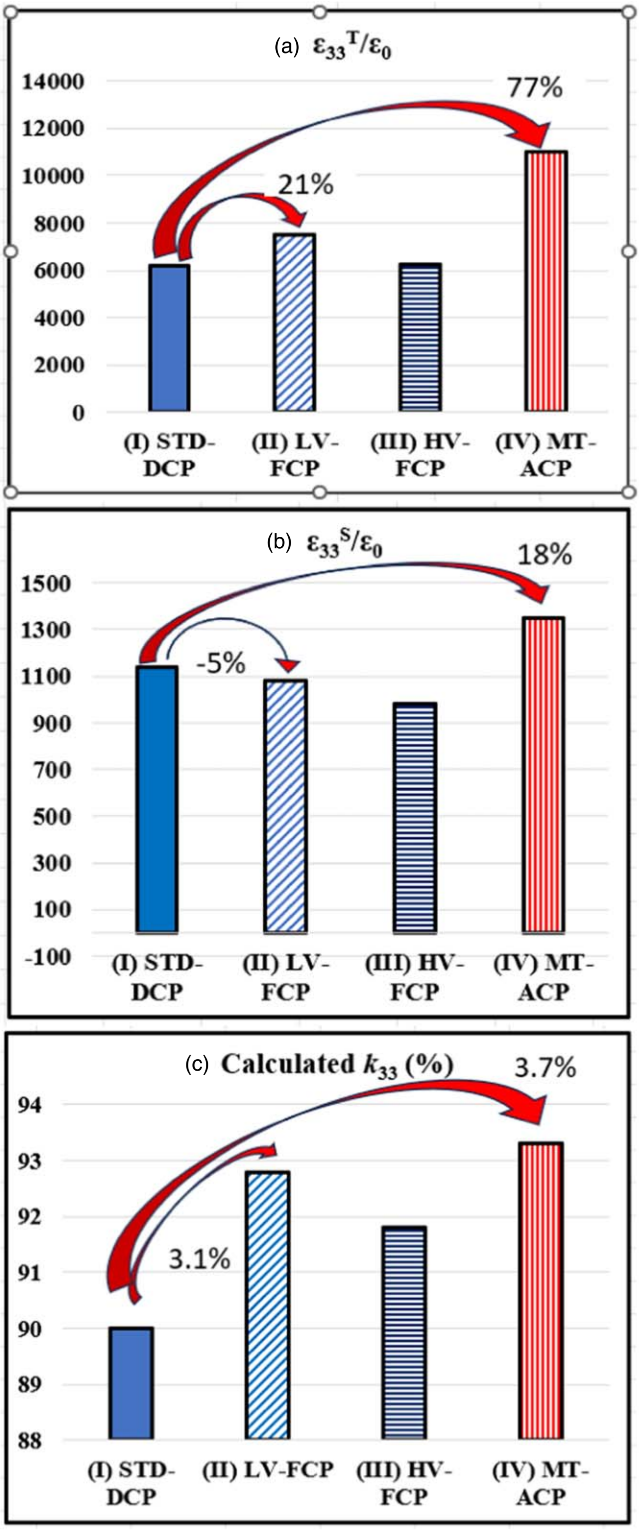

Fig. 4. (a) $\varepsilon_{33}^{T}/\varepsilon_0$, (b) $\varepsilon_{33}^{S}/\varepsilon_0$, and (c) calculated k_{33} of PMN-0.3PT SCs under different poling processes, (I)STD-DCP, (II) LV-FCP, (II) HV-FCP, and (IV) MT-ACP.

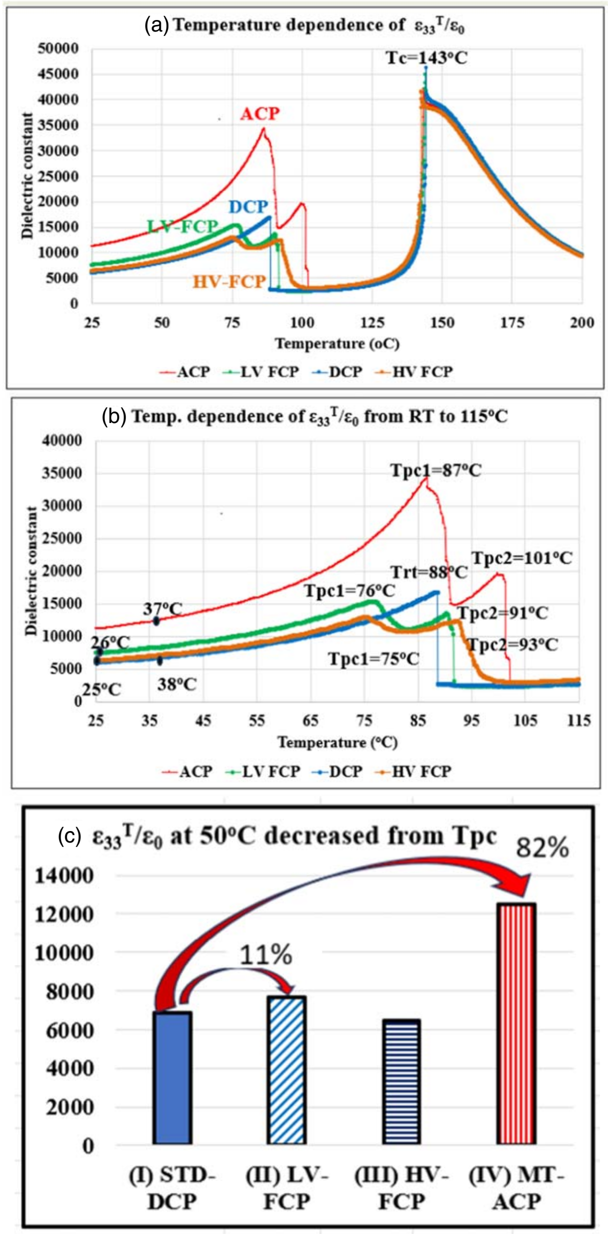

Fig. 5. Temperature dependence of $\varepsilon_{33}^{T}/\varepsilon_0$ (a) from RT to 200 °C, (b) from RT to 115 °C, and (c) $\varepsilon_{33}^{T}/\varepsilon_0$ of 50 °C decreased the temperature from the Tpc for PMN-0.3PT SCs for different poling processes, (I)STD-DCP, (II) LV- FCP, (II) HV-FCP, and (IV) MT-ACP.

61 °C, which is problematic due to its low operating temperature range. For this reason, we proposed to compare the $\varepsilon_{33}^{T}/\varepsilon_0$ of piezoelectric materials with different Tpc at a constant temperature from the Tpc, in this case 50 °C lower, in order to make a fair comparison. By comparing these values, it is possible to objectively compare the intrinsic improvement of SCs poled by various poling methods. Figure 5(a) shows the dielectric loss peak temperature (T_c) at 143 °C and maximum $\varepsilon_{33}^{T}/\varepsilon_0$ temperature (T_m) at 150 °C, which are consistent with the JFE Mineral Co. report.[36] As shown in Fig. 5(a), the rhombohedral to tetragonal phase transition (Trt) of the normal (I) STD-DCP SC was observed at Trt = 88 °C, its maximum $\varepsilon_{33}^{T}/\varepsilon_0$ was 17 000, and the RT $\varepsilon_{33}^{T}/\varepsilon_0$ was 6200. The (IV) MT-ACP SC shows two Tpcs, Tpc1 = 87 °C and Tpc2 = 101 °C, suggesting that a new phase (orthorhombic and/or monoclinic) was induced by the electric field. The maximum $\varepsilon_{33}^{T}/\varepsilon_0$ of Tpc1 was 34 000, about twice that of STD-DCP SC, and the RT $\varepsilon_{33}^{T}/\varepsilon_0$ was as large as 11 000.

Figures 5(b) and 5(c) show the $\varepsilon_{33}^{T}/\varepsilon_0$ of 50 °C decreased from the Tpc for PMN-0.3PT SCs for the four poling processes.

Figure 6 shows the d_{33} and g_{33} of the PMN-0.3PT SCs for the different poling processes. The ACP SCs showed very

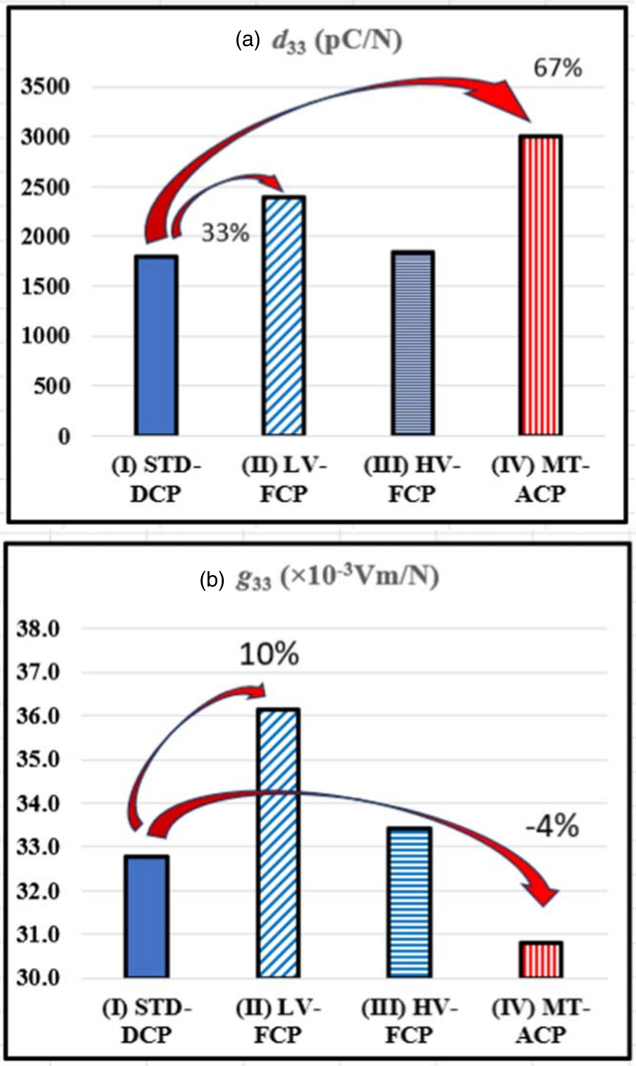

Fig. 6. (a) d_{33} and (b) g_{33} of PMN-0.3PT SCs for different poling processes, (I) STD-DCP, (II) LV-FCP, (II) HV-FCP, and (IV) MT-ACP.

high $d_{33} = 3000$ pC/N, which is a 67% enhancement compared to those of the DCP SCs. However, the ACP SC showed $g_{33} = 31 \times 10^{-3}$ Vm/N, which is 4% lower than the DCP SC of 33×10^{-3} Vm N^{-1}. However, the FCP SC showed $g_{33} = 36 \times 10^{-3}$ Vm N^{-1}, which was 10% larger than that of the DCP SC. Furthermore, over the poled conditions tested, under ACP conditions at RT, when the ACP SC was subjected to a voltage tenfold greater (35.4 kVrms cm^{-1}) than that of the MT-ACP SC, there was a discernible 26% reduction in its performance ($d_{33} = 2285$ pC/N, $\varepsilon_{33}{}^{T}/\varepsilon_0 = 8390$) due to an over-poled phenomenon,[41] but this is still higher than the (I) STD-DCP SC. These results suggest that the (II) LV-FCP SC is good for improving the receiving efficiency of transducers compared to ACP and STD-DCP SCs.

Figure 7 shows the (a) coupling factors k_t and k_{31} and (b) the frequency constants of the thickness mode N_t and length mode N_{31} of the PMN-0.3PT SCs for the four different poling processes.

The k_t for the four poling processes were almost the same, approximately 60%, but the k_{31} for FCP SCs were 53%–55%, clearly higher than those for DCP and ACP SCs, which were 45%–47%. The frequency constants N_t for the four poling processes were almost equal at about 1900 Hz·m; however,

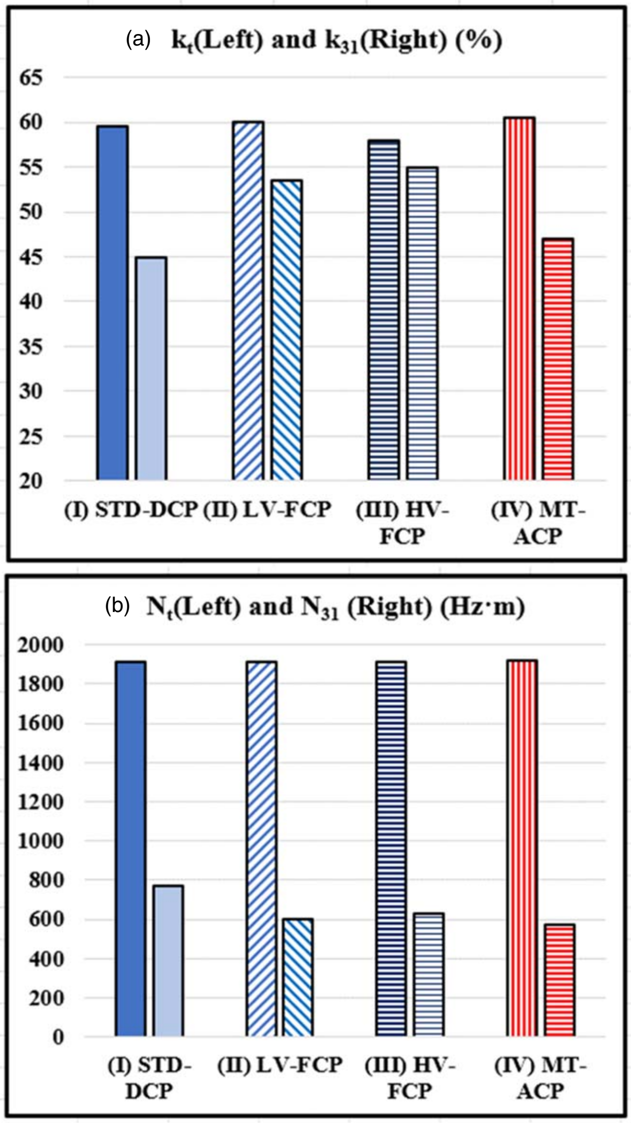

Fig. 7. (a) Coupling factors k_t and k_{31} and (b) frequency constants of the thickness mode N_t and length mode N_{31} of the PMN-0.3PT SCs for the different poling processes, (I)STD-DCP, (II) LV-FCP, (II) HV-FCP, and (IV) MT-ACP.

the N_{31} was 570 Hz·m for ACP SCs, 605 Hz·m, 630 Hz·m for LV-FCP and HV-FCP SCs, and 770 Hz·m for DCP SCs, showing a large difference. Since high k_{33} and low k_{31} are known to be effective in reducing unwanted vibrations (spurious mode vibration) in medical and underwater ultrasonic transducer applications, the ACP SC is considered to be the most useful.

In general, the $\varepsilon_{33}{}^{T}/\varepsilon_0$ and coupling factor k_{33} contribute to the piezoelectric d_{33} of piezoelectric materials at RT, as shown in Eq. (7):

$$d_{33} = k_{33}\sqrt{\varepsilon_0 \ \varepsilon_{33}{}^{T} \ S_{33}{}^{E}}, \tag{7}$$

where d_{33}, k_{33}, and $S_{33}{}^{E}$ are the piezoelectric constants, electromechanical coupling factor bar mode, and elastic compliances, respectively.

It is also known that, for relaxor-based piezoelectric SCs in the rhombohedral phase, the maximum $\varepsilon_{33}{}^{T}/\varepsilon_0$ at the Tpc contributes most to the high $\varepsilon_{33}{}^{T}/\varepsilon_0$ and d_{33} at RT.

The maximum $\varepsilon_{33}{}^{T}/\varepsilon_0$ at a 50 °C decrease from the Tpc1 was 12500 for the (IV) MT-ACP SC, followed by the (II)

LV-FCP SC, (7670), the (I) STD-DCP SC (6880), and the (III) HV-FCP SC (6470), respectively. It is important to note that the $\varepsilon_{33}{}^{T}/\varepsilon_0$ at a 50 °C decrease from the Tpc1 of the (I) STD-DCP SC (6880) is higher than the (III) HV-FCP SC (6470); even the RT value of the (I) STD-DCP SC (6200) was lower than the (III) HV-FCP SC (6250) due to a large shift of Tpc by the applied DC voltage.

Lin et al. reported that a 0.1 mm thick sample of PMN-PT had a $\varepsilon_{33}{}^{T}/\varepsilon_0$ of 3000 and $d_{33} = 1300$ pC/N when FCP was performed at RT.[19] However, when this sample was subjected to FCP at 6 kV cm^{-1}, a higher $\varepsilon_{33}{}^{T}/\varepsilon_0$ of 5600 and d_{33} of 2200 pC N^{-1} were obtained, representing an improvement of 87% and 69%, respectively. However, their experimental results offer limited information, and there are several aspects that warrant further investigation.

It should be noted that the PMN-PT SC samples used in Lin et al. were prepared by the OC-BM method, which has poor uniformity of composition and properties, and there is a large variation in properties among the samples. Furthermore, the exact amount of PT content is not given.

Secondly, the comparison of DCP and FCP was performed in Lin et al. by only using samples with a thickness of 0.1 mm. The piezoelectric and dielectric properties of SCs with a thickness of about 0.1 mm are strongly influenced processing damage to the surface layer. Recently, Takahashi and Namba reported that moderate heat treatment is essential to obtain good properties for PMM-PT SCs with a thickness of 0.1 mm or less because the $\varepsilon_{33}{}^{T}/\varepsilon_0$ is strongly affected by processing damage.[45,46]

Finally, the data of $\varepsilon_{33}{}^{T}/\varepsilon_0$ temperature dependence of DCP and FCP SCs samples were not disclosed in Lin et al. Therefore, it is not possible to accurately determine whether the large $\varepsilon_{33}{}^{T}/\varepsilon_0$ at RT is due to the decrease in Tpc. Wan et al. reported that the Trt decreased by 27 °C (from 80 °C to 53 °C) when the FCP was from 250 °C to RT by applying 3 kV cm^{-1} for 0.24PIN-0.46PMN-0.30PT SCs.[47] The result is similar to our PMN-0.3PT SC in these experimental results.

In our experiments, we used four different poling methods on 19 pieces of PMN-30PT SC plates prepared by the CF-BM method, which guarantees a high degree of uniformity in composition and properties. A thickness of about 0.5 mm was also used, which provides stable properties. Furthermore, the $\varepsilon_{33}{}^{T}/\varepsilon_0$ temperature dependences were precisely measured, and the $\varepsilon_{33}{}^{T}/\varepsilon_0$ was decreased by 50 °C from the Tpc, which eliminates the effect of $\varepsilon_{33}{}^{T}/\varepsilon_0$ improvement at RT, which was defined as $\varepsilon_{33}{}^{T}/\varepsilon_0$ at a 50 °C decrease from the Tpc, and this value is shown in Fig. 5(c). From this result, the $\varepsilon_{33}{}^{T}/\varepsilon_0$ improvement of (II) LV-FCP over (I) STD-DCP was as large as 11%, but was smaller than that of (IV) MT-ACP, which was 82%. The reliability of the effects of our four poling methods on piezoelectric and dielectric properties is considered to be extremely high.

Figure 8 shows scanning electron microscopy (SEM) microstructures of the (I) STD-DCP SC, (II) LV-FCP SC, (III) HV-FCP SC, and (IV) MT-ACP SC used in this experiment. These poled SC samples were broken manually and the fresh surface of the center portion was observed.[22] It is clear from this figure that (I) STD-DCP SCs have a low RT $\varepsilon_{33}{}^{T}/\varepsilon_0$ of 6000–7500 and Tpc $\varepsilon_{33}{}^{T}/\varepsilon_0$ of 12 000–17 000. The (II) LV-FCP SCs have a microstructure with a mixture of small and random, 79° and 109° domains similar to depolarized DEP SCs.[20,22] The (IV) MT-ACP SCs with high RT $\varepsilon_{33}{}^{T}/\varepsilon_0$ of 11 000 and Tpc $\varepsilon_{33}{}^{T}/\varepsilon_0$ of 34 000 showed distinct 109° domain layers with a width of several μm parallel to the electrode (perpendicular to the electric field).[20,22,23] These 0.5–5 μm aligned 109° domain layers parallel to the electrode are similar to those observed in previous ACP SCs.[20,22–25,33] These fine domain layers parallel to the electrode in PMN-PT SCs are unique to the ACP process, and it is believed that the 109° domain layer of appropriate width contributes to the large

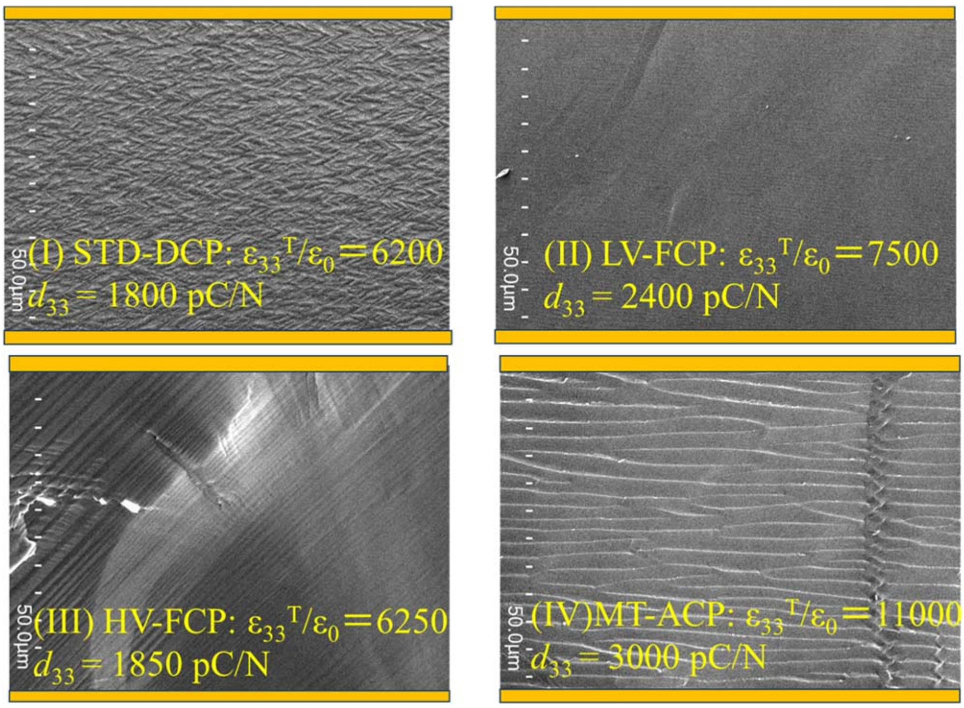

Fig. 8. SEM microstructures of PMN-PT SCs for different poling processes, (I) STD-DCP, (II) LV-FCP, (III) HV-FCP, and (IV) MT-ACP. Note that the gold top and bottom lines are electrodes and the image area is 60 × 90 μm.

$\varepsilon_{33}{}^{T}/\varepsilon_0$ and d_{33} of PMN-PT SCs. This fact has been reported by many researchers.[20,31,33] Furthermore, unlike all other SCs, the (III) HV-FCP SCs exhibit a complex and nonuniform domain structure that is nonparallel to the electrode. This is the inhomogeneous domain structure of PMN-PT SCs caused by over-poling, and the $\varepsilon_{33}{}^{T}/\varepsilon_0$ is almost the same as that of the STD-DCP SC.[35,41,48]

Furthermore, as shown in Fig. 5(b), the STD-DCP SC was the only one that exhibited a rhombohedral to tetragonal phase transition point Trt of 88 °C. On the other hand, the MT-ACP SC showed complicated phase transition from a rhombohedral phase to a tetragonal phase via a monoclinic and/or orthorhombic phase at 87 °C and 101 °C.[49] This complicated phase transition[50] and the appearance of 109° layers domain morphology in the ACP process may contribute to the high dielectric and piezoelectric properties of PMN-PT SCs.[20,21,29,33,49]

4. Conclusions

We have investigated the effectiveness of poling processes and systematic comparisons for PMM-0.3PT SCs prepared by the CF-BM method with high compositional and property uniformity using four processes, (I) STD-DCP, (II) LV-FCP, (III) HV-FCP, and (IV) MT-ACP. The highest $\varepsilon_{33}{}^{T}/\varepsilon_{0,}$ calculated $k_{33,}$ and d_{33} were obtained by the MT-ACP SC ($\varepsilon_{33}{}^{T}/\varepsilon_0 = 11\ 000$, $k_{33} = 93.3\%$, and $d_{33} = 3000$ pC/N), followed by the LV-FCP SC ($\varepsilon_{33}{}^{T}/\varepsilon_0 = 7500$, $k_{33} = 92.8\%$, $d_{33} = 2400$ pC/N), HV-FCP ($\varepsilon_{33}{}^{T}/\varepsilon_0 = 6250$, $k_{33} = 91.8\%$, $d_{33} = 1850$ pC/N), and STD-DCP ($\varepsilon_{33}{}^{T}/\varepsilon_0 = 6200$, $k_{33} = 90\%$, $d_{33} = 1800$ pC/N). The LV-FCP SC showed a 21%, 3.1%, and 33% increase in $\varepsilon_{33}{}^{T}/\varepsilon_{0,}$ k_{33}, and d_{33} compared to the STD-DCP SC, respectively; however, this was not as much as the 77%, 3.7%, and 67% improvement of the MT-ACP SC. In addition, the FCP SCs exhibited a decrease in Tpc of about 10 °C compared to other DCPs and ACP SCs, which contributes to their large $\varepsilon_{33}{}^{T}/\varepsilon_0$ at RT. These fine domain layers parallel to the electrode in PMN-PT SCs are unique to the ACP process, and it is believed that the fine 109° domain layers of appropriate width, 0.5 to 5 μm, contributes to the large $\varepsilon_{33}{}^{T}/\varepsilon_0$ and d_{33} of PMN-PT SCs. These results provide good guidance for the design of various piezoelectric transducers and devices based on PMN-PT SCs.

Acknowledgments

This work was supported by Office of Naval Research (ONR) under Grant # N00014-21-1-2058 and the Murata Science Foundation 2023.

ORCID iDs

Hiroshi Maiwa https://orcid.org/0000-0002-8034-4553

1) S. Saitoh, M. Izumi, S. Shimanuki, S. Hashimoto, and Y. Yamashita, U.S. Patent 5295487 (1994).
2) Nava Setter, *Piezoelectric Materials in Devices: extended reviews on current and emerging piezoelectric materials, technology, and applications* (Ecole Polytechnique fédérale de Lausanne, Lausanne 1015, Switzerland, 2002) p. 1.
3) X. Jiang, J.-W. Kim, and K.-R. Kim, Crystals **4**, 351 (2014).
4) Z.-G. Ye, "Chap. 3 Recent developments and applications of piezoelectric crystals, Handbook of dielectric, piezoelectric and ferroelectric materials: synthesis, properties and applications (Woodhead Publishing Materials, England, 2008) p. 73.
5) S. Zhang, F. Li, F. Yu, X. Jiang, H.-Y. Lee, J. Luo, and T. R. Shrout, J. Korean Ceram. Soc. **55**, 419 (2018).
6) K. Uchino, "'Part II Preparation methods and applications, advanced piezoelectric materials," *Sci. Technol.* (A volume in Woodhead Publishing in Materials, England, 2017) 2nd ed.
7) Y. Yamashita, T. Karaki, H.-Y. Lee, H. Wan, H.-P. Kim, and X. Jiang, IEEE Trans. Ultrason. Ferroelectr. Freq. Control **69**, 3048 (2022).
8) H. Luo, G. Xu, H. Xu, P. Wang, and Z. Yin, Jpn. J. Appl. Phys. **39**, 5581 (2000).
9) T. Karaki, M. Adachi, Y. Hosono, and Y. Yamashita, Jpn. J. Appl. Phys. **41**, L402 (2002).
10) S. Zhang and F. Li, J. Appl. Phys. **111**, 031301 (2012).
11) K. Echizenya and M. Matsushita, "Continuous feed growth and characterization of PMN-PT single crystals," 2011 IEEE Int. Ultrasonics Symp., Orlando, FL, 2011, p. 1813.
12) K. Echizenya, K. Nakamura, and K. Mizuno, J. Cryst. Growth **531**, 125364 (2020).
13) K. Echizenya, N. Noda, and H. Noro, Crystals **12**, 1183 (2022).
14) Y. Sun, Y. Ota, H.-P. Kim, H. Wan, Y. Yamashita, T. Karaki, and X. Jiang, IEEE Trans. Ultrason. Ferroelectr. Freq. Control **69**, 3087 (2022).
15) Y. Sun, Y. Ota, T. Fujii, Y. Yamashita, H.-P. Kim, H. Wan, X. Jiang, and T. Karaki, Jpn. J. Appl. Phys. **61**, SN1026 (2022).
16) K. Echizenya and K. Noda, Jpn. J. Appl. Phys. **62**, SM1023 (2023).
17) J. Kuwata, K. Uchino, and S. Nomura, Jpn. J. Appl. Phys. **21**, 1298 (1982).
18) T. R. Shrout, Z. P. Zung, N. Kim, and S. Markgraf, Ferroelectr. Lett. Sect. **12**, 63 (1990).
19) D. Lin, H.-J. Lee, S. Zhang, F. Li, Z. Li, Z. Xu, and T. R. Shrout, Scr. Mater. **64**, 1149 (2011).
20) N. Yamamoto, Y. Yamashita, Y. Hosono, K. Itsumi, and K. Higuchi, U.S. Patent 0062261 A1 (2014).
21) Y. Yamashita, N. Yamamoto, Y. Hosono, and K. Itsumi, U.S. Patent 0372219 A1 (2015).
22) W.-Y. Chang, C.-C. Chung, C. Luo, T. Kim, Y. Yamashita, J. L. Jones, and X. Jiang, Mater. Res. Lett. **6**, 537 (2018).
23) C. He, T. Karaki, X. Yang, Y. Yamashita, Y. Sun, and X. Long, Jpn. J. Appl. Phys. **58**, SLLD06 (2019).
24) Y. Sun, T. Fujii, T. Karaki, and Y. Yamashita, Jpn. J. Appl. Phys. **58**, SLLC06 (2019).
25) C. Qiu et al., Nature **577**, 350 (2020).
26) J. Xu et al., Appl. Phys. Lett. **116**, 202903 (2020).
27) Z. Zhang, J. Xu, S. Liu, J. Xiao, X. Wang, Z. Liang, and H. Luo, Ultrasonics **108**, 106175 (2020).
28) M. Ma, S. Xia, K. Song, H. Guo, S. Fan, and Z. Li, J. Appl. Phys. **127**, 064106 (2020).
29) Y. Sun, T. Karaki, Z. Wang, T. Fujii, and Y. Yamashita, Jpn. J. Appl. Phys. **60**, SFFC04 (2021).
30) H. Wan, C. Luo, C. Liu, W.-Y. Chang, Y. Yamashita, and X. Jiang, Acta Mater. **208**, 116759 (2021).
31) Y. Sun, T. Karaki, and Y. Yamashita, Jpn. J. Appl. Phys. **61**, SB0802 (2022).
32) Z. Wang, Y. Yamashita, C. Luo, Y. Sun, T. Karaki, and T. Fujii, Jpn. J. Appl. Phys. **61**, SN1009 (2022).
33) H.-P. Kim, H. Wan, C. Luo, Y. Sun, Y. Yamashita, T. Karaki, H.-Y. Lee, and X. Jiang, IEEE Trans. Ultrason. Ferroelectr. Freq. Control **69**, 3037 (2022).
34) M. Liu, H. Tang, W. Zhang, Z. Wang, X. Yang, R. Su, X. Long, and C. He, IEEE Trans. Ultrason. Ferroelectr. Freq. Control **69**, 3081 (2022).
35) H. Wan, C. Luo, H.-P. Kim, C. C. Chung, Y. Yamashita, and X. Jiang, Appl. Phys. Lett. **120**, 192901 (2022).
36) Y. Liu, Q. Li, L. Qiao, Z. Xu, and F. Li, Adv. Sci. **9**, 2204631 (2022).
37) Y. Wang, Y. Wang, P. Yan, P. Guo, Y. Zhang, and Y. Qin, Appl. Phys. Express **16**, 011003 (2023).
38) Y. Guan, H. Hang, D. Lin, X. Wang, Y. Tang, and H. Luo, Sens. Actuators A: Phys. **354**, 114275 (2023).
39) Y. Yamashita, H. Sun, Y. Xiang, H. Maiwa, H.-Y. Lee, H.-P. Kim, and X. Jiang, Jpn. J. Appl. Phys. **62**, SM1009 (2023).

40) Y. Xiang, Y. Sun, Y. Yamashita, T. Karaki, and H. Maiwa, Jpn. J. Appl. Phys. **62**, SM1009 (2023).
41) Y. Xiang, Y. Sun, Y. Yamashita, T. Karaki, and H. Maiwa, J. Ceram. Soc. Jpn, **131**, 263 (2023).
42) H. Tang, W. Zhang, X. Yang, Z. Wang, R. Su, Y. Liu, X. Long, and C. He, Curr. Appl Phys. **55**, 75 (2023).
43) Y. J. Yamashita, Y. Yamagata, Y. Xiang, H. Sun, H. Maiwa, H.-P. Kim, and X. Jiang, Abstract of the 44th Symp. on UltraSonic Electronics (USE) Toyama2023.
44) "IEEE Standard for relaxor-based single crystals for transducer and actuator application#1859 (2017).
45) H. Takahashi, H. Suzuki, and Y. Namba, CIRP Ann. **65**, 541 (2016).
46) T. Namba, A. Tanaka, T. Sato, and Y. Sakano, Jpn. J. Appl. Phys. **62**, SM1016 (2023).
47) Y. Wan, Z. Li, S. Fan, Z. Xu, and Y. Xi, Ferroelectrics **456**, 8 (2013).
48) L. C. Lim, M. Shanthi, K. K. Rajan, and C. Y. Lim, J. Cryst. Growth **282**, 330 (2005).
49) C. Que, Z. Xue, Z. An, J. Liu, G. Zhang, S. Zhang, L. Q. Chen, and F. Li, Acta Mater. **210**, 116853 (2020).
50) F. Li et al., Science **364**, 264 (2019).